



UV-LED/ilmenite/persulfate for azo dye mineralization: The role of sulfate in the catalyst deactivation

Jefferson E. Silveira ^{a,*}, Wendel S. Paz ^{b,*}, Patricia Garcia-Muñoz ^a, Juan A. Zazo ^a, Jose A. Casas ^a

^a Chemical Engineering, Autonomous University of Madrid, Cantoblanco, 28049 Madrid, Spain

^b Department of Condensed Matter Physics, Autonomous University of Madrid, Cantoblanco, 28049 Madrid, Spain

ARTICLE INFO

Article history:

Received 6 April 2017

Received in revised form 3 July 2017

Accepted 24 July 2017

Available online 1 August 2017

Keywords:

Ilmenite

UV-LED

Persulfate

Deactivation

DFT

ABSTRACT

This work investigates the effect of UV-LED on the persulfate (PS) activation with natural ilmenite (FeTiO_3) in the oxidation of azo dye Disperse Blue 3 (DB3). The high induction period and the scarce ability of this mineral to activate PS can be overcome by using UV irradiation to increase the $\text{SO}_4^{\bullet-}$ generation via photoreduction of $\text{Fe}(\text{III})$ to $\text{Fe}(\text{II})$ on the ilmenite surface, main responsible of $\text{SO}_4^{\bullet-}$ formation in iron-based catalysis. The effect of several operating conditions such as persulfate dose (20–100% of the theoretical stoichiometric amount), reaction temperature (30–70 °C) and mineral concentration 320 mg L⁻¹ has been studied. Under optimum conditions (320 mg L⁻¹ of ilmenite, pH₀: 3, using 100% of stoichiometric amount of PS at 70 °C under UV-LED radiation) more than 95% TOC reduction and 92% PS decomposition were reached after 180 min. The progressive deactivation of FeTiO_3 through successive experiments can be explained, according to density functional theory (DFT) calculations, by the formation of a passivation layer due to adsorption of SO_4^{2-} on the FeTiO_3 surface.

© 2017 Elsevier B.V. All rights reserved.

1. Introduction

The growth in the use of synthetic dyes has been accompanied by large volumes of industrial effluent causing environmental damage to the living organisms [1]. There are several types of synthetic dyes which are widely used in paper, cosmetics, food, pharmaceutical and textile industries [2,3]. Among them, azo dyes are the most common used in textile industry, representing about 70% of all commercial dyes. These compounds contain an azo group (—N=N—) as chromophore, associated with aromatic systems linked to other groups such as —OH and —NO₂ [4,5].

Advanced oxidation processes (AOP's) based on the in situ hydroxyl radical (HO^{\bullet}) generation have been widely used as a feasible way to mineralize azo dyes. Electrochemical oxidation [6], solar photoelectro-Fenton [7], photocatalytic degradation [8] and ozonation [9] represent some of those alternatives to HO^{\bullet} generation.

Activated persulfate based AOP's constitutes an alternative to the aforementioned procedures. The persulfate anion (PS) is a strong oxidant, with a redox potential of 2.01 V [10]. Further-

more, PS can be induced to generate a stronger sulfate radical ($\text{SO}_4^{\bullet-}$), with a standard redox potential varying between 2.5 and 3.1 V [11]. Many studies have demonstrated the oxidation of azo dyes by activated persulfate. Frontistis et al. [12] demonstrated the effectiveness of using PS/UV for methyl orange decolorization. Kordkandi and Forouzesh [13] have applied thermally activated persulfate to treat aqueous methylene blue. Xu and Li [14] reported the degradation of azo dye Orange G by Fe^{2+} activated persulfate. In addition, Teel et al. [15] compared the activation of persulfate with 13 naturally occurring minerals found in surface and subsurface soils, for in situ chemical oxidation, among them cobaltite, pyrite, siderite and ilmenite. However, those results revealed a scarce ability to decompose persulfate in a natural groundwater system.

Ilmenite (FeTiO_3) as a titanate of ferrous iron mineral, is an anti-ferromagnetic semiconductor, with a band gap varying between 2.4 and 2.9 eV with potential applications in chemical catalysts and photocatalysts reactions [16–18]. At room temperature and atmospheric pressure, FeTiO_3 adopts an ordered corundum structure [8,9] of space group $R\bar{3}$, in which $\text{Fe}(\text{II})$ and $\text{Ti}(\text{IV})$ form alternating layers along the rhombohedral axis of the crystal, with oxygen layers between them. Layers of Fe and Ti alternate with a cation ordering of Ti-Fe-V-Fe-Ti (V: vacant sites) along the c axis.

So far, the application of ilmenite as catalyst in AOP's processes is limited by a high induction period and a low activity [19]. These

* Corresponding authors.

E-mail addresses: jeffersonano@gmail.com (J.E. Silveira), wpascal1@gmail.com (W.S. Paz).

drawbacks can be overcome by using UV irradiation to improve the efficiency via photoreduction of Fe(III) to Fe(II) in the ilmenite surface, decreasing the induction period [20,21]. In this sense, Fe(II) plays an important role in SO_4^{2-} generation in iron-based catalysis. Liang et al. [22] found that Fe (II), but not Fe(III), activates PS. Light emitting diodes (LEDs) have become an alternative to conventional UV sources [21] due to a higher current-to-light conversion efficiencies, compactness, suitability for periodic illumination, narrow band emission, no disposal problems and long life [23,24].

This work outlines the combination of temperature and UV LED radiation (λ : 400–405 nm) with the aim of improving catalytic properties of ilmenite mediated activation of persulfate toward textile dye DB3 mineralization, allowing the use of this raw mineral as an inexpensive and sustainable catalyst.

The anthraquinone azo dye DB3 ($\text{C}_{17}\text{H}_{16}\text{N}_2\text{O}_3$) has been chosen as a target compound because of their toxic and mutagenic characteristics [25]. The contribution of sulfate upon the FeTiO_3 surface passivation during PS activation has been also studied by performing *ab initio* band calculations based on the density functional theory using the plane-wave pseudopotential method as implemented in Quantum Espresso code.

2. Material and methods

2.1. Reactants

Disperse blue 3 was provided by Sigma Aldrich (dye content 20%). The simulated disperse azo dye aqueous solution was prepared by complete dissolving 80 mg (16 mg of dye) in 1 L deionized water. The average COD of the resulting solution was 112 mg L^{-1} (measured in triplicate). Persulfate (98%) was purchased from Panreac (Spain). The chemicals used either as potassium iodide (KI) (99%), sodium carbonate (Na_2CO_3) (99%), sodium bicarbonate (NaHCO_3) (99.7%), sodium sulfate (Na_2SO_4) (99%), dichloromethane (CH_2Cl_2) (99.8%), *tert*-butyl alcohol (TBA), (99.5%), ethanol (EtOH) (95%) were purchased from Sigma-Aldrich (U.S.A). The ilmenite (Ref. 50110700) was provided by Marphil S.L. (Spain). Titanium dioxide (TiO_2) was purchased from Degussa Corporation.

2.2. Ilmenite characterization

Experimental band-gap determination was carried out plotting $(\alpha h\nu)^n$ versus $h\nu - E_g \pm E$ (Ω) (where $n=2$ for indirect semiconductors) giving a linear absorption edge and its cut with base line corresponds to band-gap energy. The diffuse reflectance spectra were recorded with a UV-vis Agilent Varian, Cary 5000. The iron and titanium content of fresh and used ilmenite was determined by total reflection X-ray fluorescence, using a TXRF spectrometer 8030c (detection limit 0.007 and 0.02 mg L^{-1} for Fe and Ti respectively). The crystalline phases in the catalyst were analyzed by X-ray diffraction (XRD) using a Siemens model D-5000 diffractometer with $\text{Cu K}\alpha$ radiation ($\lambda = 1.54 \text{ \AA}$). Ilmenite was characterized by X-ray Photoelectron Spectroscopy (XPS) with a $\text{K}\alpha$ Thermo Scientific apparatus with an $\text{Al K}\alpha$ ($h\nu = 1486.68 \text{ eV}$) X-ray source using a voltage of 12 kV under vacuum ($2 \times 10^{-7} \text{ mbar}$) condition. For the peak analysis a Shirley type background was used. Peaks were fitted with Gaussian and Lorentzian functions using the XPS Peak 4.1 software [26]. The BET specific surface area (S_{BET}) of the catalyst was characterized from nitrogen adsorption-desorption isotherms at 77 K using a Micromeritics Tristar 3020 apparatus. The samples were previously outgassed overnight at 150°C to a residual pressure of 10^{-3} Torr [21].

2.3. DFT model setup and calculations methods

The first-principle calculations were carried out based on the frame-work of density functional theory (DFT), as implemented in the Quantum ESPRESSO package [27]. The generalized gradient approximation of Perdew-Burke-Ernzerhof (GGA-PBE) [28] was adopted for exchange-correlation functional. Since GGA-PBE functionals usually underestimate the band gaps, fail to correctly treat *d* orbitals in transition-metal oxides due to unphysical self-interaction and GGA-PBE incorrectly predict a metallic state, we use here the hybrid nonlocal exchange-correlation functional (HSE06) [29] in an attempt to get more reliable values, possibly closer to the experimental ones.

The HSE functional, with its fraction of screened short-ranged Hartree-Fock exchange, yields reasonably accurate predictions for energy band gaps in semiconductors [30,31]. The electron-ion interaction is described using the norm-conserving Troullier-Martins pseudopotentials [32] are employed in PBE and HSE calculations. The energy cut-off for the plane wave basis set is put at 100 Ry with a charge density cut-off of 400 Ry. We have used a Monkhorst-Pack [32] scheme with a $6 \times 6 \times 3$ k-mesh for the Brillouin zone integration.

The complete hexagonal unit cell of FeTiO_3 ilmenite is shown in Fig. 2. All calculations were carried out under rhombohedral symmetry constraints. The FeTiO_3 was simulated in the supercell approach under structure optimizations based on the experimental lattice structure obtained from the American Mineralogist Crystal Structure Database [33].

2.4. Typical reaction procedure

The UV-LED system consisted of a glass jacketed batch reactor (the reaction volume was set at 250 mL) placed in a magnetic stirrer (200 rpm). A commercial LED strip (SMD 5050) which radiates at 405 nm was placed around the external wall of the reactor. The irradiance corresponding to LED radiation was 10 W m^{-2} with a power of 19 W. The reaction temperature was controlled between 30 and 70°C with a thermal batch recirculation system (Julabo 13) (Fig. S1). The PS dose was varied between 20% (0.34 g L^{-1}) and 100% (1.7 g L^{-1}) of the stoichiometric theoretically needed for complete mineralization of COD (12 g PS/g COD). The ilmenite concentration was 320 mg L^{-1} (preliminary studies showed that the higher amounts not increase the reaction rate). The reusability of ilmenite was appraised in three successive experiments. The catalyst recovered by filtration and dried overnight at 60°C after each run.

2.5. Analytical methodology

Reaction samples were instantly placed in an ice bath and immediately analyzed after centrifugation at 3500 rpm for 10 min. The mineralization degree of DB3 was determined measuring the total organic carbon (TOC) by TOC-V CSH, Shimadzu, Japan. A gas chromatography-mass spectrometry (GC-MS) system in electron impact ionization mode was used for the aromatic by-products with a CP-3800/Saturn 2200, Varian, equipped with an automatic injector CP-8200/SPME, solid-phase micro extraction [34]. Short-chain organic acids were analyzed by ion chromatography with chemical suppression (Metrohm 790 IC) using a conductivity detector. A Metrosep A supp 5-250 column (25 cm length, 4 mm diameter) was used as stationary phase and an aqueous solution containing $3.2 \text{ mM Na}_2\text{CO}_3$ and 1 mM NaHCO_3 was used as the mobile phase at a flow rate of 0.7 mL min^{-1} [21]. The residual PS was determined by colorimetric method [35]. The iron released from the ilmenite was measured by inductively coupled plasma optical emission spectroscopy (ICP-OES) using an ICP-MS Elan 6000 PerkinElmer Scieix (with detection limit of 0.045 ppb). The acute

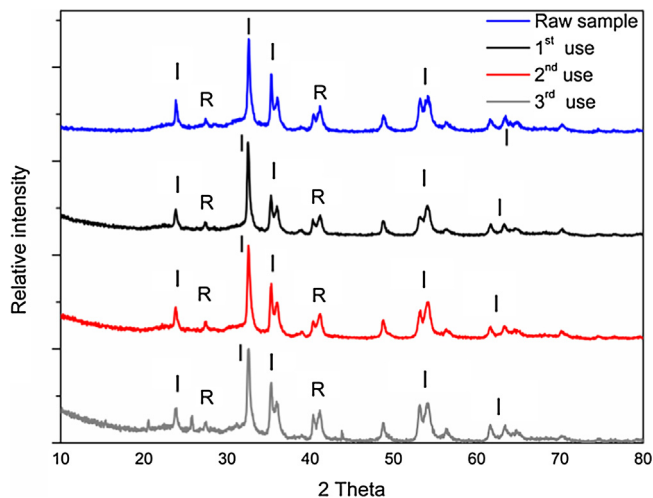


Fig. 1. Normalized XRD of ilmenite before and after three uses.

toxicity measurements were carried out by the brine shrimp *A. salina* bioassays, in triplicates, during 24 h, and then the LC₅₀ was calculated, according to the methodology suggested by Vanhaecke et al. [36].

3. Results and discussion

3.1. Ilmenite characterization

Ilmenite was characterized by a low surface area and a band-gap value of 2.4 eV, with a Fe(II)/Fe(III) ratio on the surface of 0.66. A more detailed characterization can be found elsewhere [16,19,20].

Fig. 1 shows the XRD of the raw ilmenite. For the sake of comparison, this figure also includes the XRD of ilmenite after each use. The weak peaks of 2-Theta = 23.9°, 32.65°, 35.3°, 40°, 48°, 53°, 61°, 63° and 27°, 36°, 41°, 54° and 57° in XRD spectrum indicates the existence of ilmenite and rutile phase, respectively, which is in agreement with the JCPDS card no. 21-1276 and 29-0733 standard data in a proportion 85/15 [19]. The Fe and Ti content (weight percentage) in raw ilmenite was 36% and 37%, respectively (measured by TXRF). The S_{BET} of the ilmenite was found to be 6 m² g⁻¹.

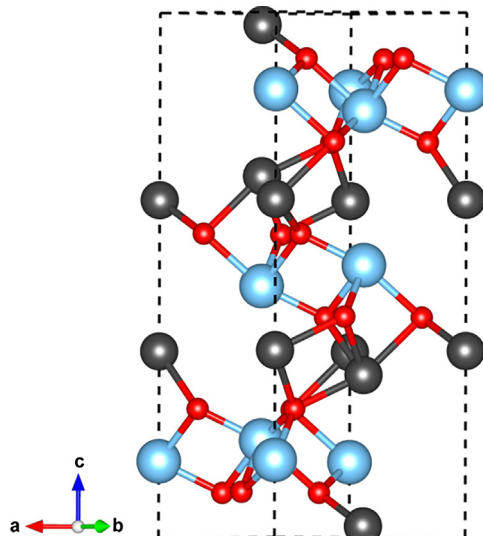


Fig. 2. FeTiO₃ surface Ti (blue), Fe (black) and O (red). (For interpretation of the references to colour in this figure legend, the reader is referred to the web version of this article.)

Table 1

Persulfate activation at different process and pseudo 1st order kinetic rate constant of TOC removal.

Reaction	Treatment	Mineralization (%)	$k_{\text{obs}} \times 10^{-3} (\text{min}^{-1})$	R ²
1	Ilmenite	<1	–	–
2	UV-LED	<1	–	–
3	Ilmenite/UV-LED	2.3	0.2	0.98
4	PS	39	3.2	0.98
5	PS/ilmenite	55	4.5	0.98
6	PS/UV-LED	51	4.2	0.97
7	PS/UV-LED/ilmenite	96	13.2	0.98
8	TiO ₂	18	1.05	0.98
9	PS/TiO ₂	63	5.3	0.97
10	PS/UV-LED/TiO ₂	82	8.8	0.98

Experimental Conditions: [DB3]₀ = 80 mg L⁻¹, [PS]₀ = 7 mM, [catalyst]₀ = 320 mg L⁻¹, UV-LED radiation = 405 nm, T = 70 °C and pH₀ = 3.

3.2. DFT model setup

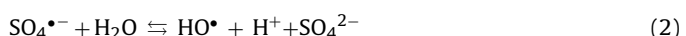
The complete hexagonal unit cell of ilmenite is presented in Fig. 2. The calculated lattice parameters for FeTiO₃ are a = b = 5.143 Å and c = 13.98 Å, which is in good agreement with the experiment data, in which a = b = 5.087 Å and c = 14.013 Å [33].

In order to gain insight into the material electronic properties, we first compute the band structure based on the crystal structure described above. For the bulk crystal, using the standard generalized gradient approximation (GGA) to the functional, we obtain an indirect band gap of 1.68 eV that increases to 2.2 eV using HSE06. These results can be compared with the electronic bandgap experimental data on bulk FeTiO₃ crystals, where we observe an electronic band gap of ~2.4 eV, which is in good agreement with the values reported in the literature for ilmenite (between 2.4 and 2.9 eV) [19,37,38].

3.3. UV-LED assisted PS/Ilmenite activity

In order to evaluate the synergistic effects of reaction temperature, UV light and ilmenite upon the PS activation and, therefore, mineralization of DB3, a set of experiments with and without UV-LED radiation were performed with the temperature ranging from 30 to 70 °C (Fig. 3). Table 1 gathers the results of previous tests performed to assess the contribution of adsorption and photolysis in absence of PS. They showed a negligible adsorption on ilmenite surface (Reaction (1)), photolysis reactions (Reaction (2)) and photocatalytic activity at 405 nm UV-LED (Reaction (3)), yielding TOC reduction lower than 2.5% after 180 min reaction time.

A variety of factors might be expected to have influence on the PS activation process (heat and metal ion-catalyzed conditions). Persulfate can be heat-activated according Eq. (1) [39]. Furthermore, the hydroxyl radicals (HO[•]) and peroxymonosulfate oxidant (HSO₅[–]) can be generated involving the reaction between SO₄^{2–} and H₂O (Eq. (2)) and the chain of reactions involving the radicals SO₄^{2–} and HO[•] respectively (Eq. (3)) [39].



In absence of both irradiation and ilmenite, the heat-activation of PS was scarce below 50 °C. Nevertheless, the DB3 mineralization steeply increased up to 39% as temperature raised up to 70 °C (Reaction (4)). The addition of ilmenite, as a source of Fe(II), promotes the heterogeneous activation of PS to produce SO₄^{2–} (Eqs. (4) and (5)) [40,41] and, therefore, the TOC removal (Fig. 3). Working at 70 °C, TOC removal was close to 55% in the system PS/ilmenite (Reaction (5)), around 16% above the mineralization achieved by

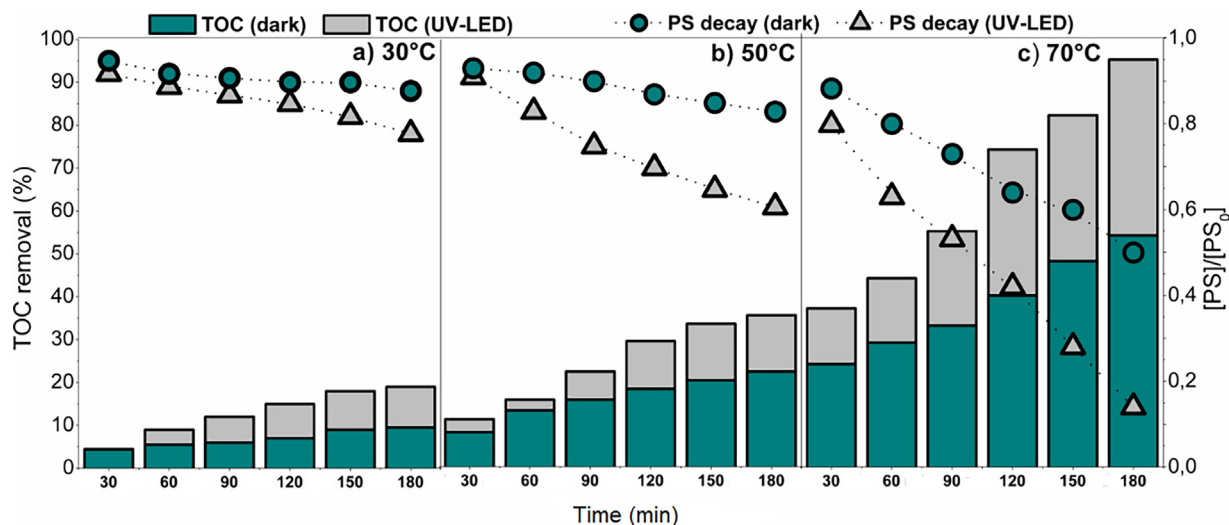
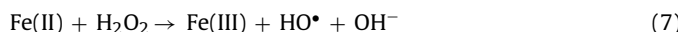
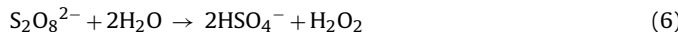
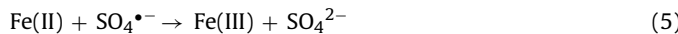
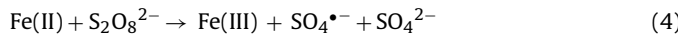


Fig. 3. Time evolution of TOC removal and PS converted with and without UV-LED radiation at 30 °C (a) 50 °C (b) and 70 °C. Experimental Conditions: $[DB3]_0 = 80 \text{ mg L}^{-1}$, $[PS]_0 = 100\%$, $[FeTiO_3]_0 = 320 \text{ mg L}^{-1}$ and $pH_0 = 3$.

heat-activation of PS, corroborating the synergistic effect of combining an iron source and temperature. Preliminary experiments showed that, in the range of initial pH amid 3 and 9, the mineralization degree of DB3 decreased as the initial pH value increased, from 95% at $pH_0: 3$ to less than 80% at $pH_0: 9$. This can be explained by the basic surface properties of ilmenite which favors the interaction between ilmenite and PS at acidic pH [16]. Besides under these conditions, both the formation of SO_4^{2-} can be catalyzed by protons [42] and the hydrolysis of PS could provoke the formation of H_2O_2 (Eq. (6)), which may lead to the generation of HO^\bullet in the presence of Fe(II) (Eq. (7)) [43].



UV-LED radiation also plays a key role in the PS activation (Eq. (8)) [44]. Rasoulifard et al. [24] demonstrated that PS can be activated using UV-LED with emission wavelengths at 360 nm on the degradation of Direct Red 23 dye. In our case, the UV-LED assisted PS activation (Table 1) enhanced in 12% the mineralization degree (Reaction (6)) comparing to the sole heat-activation at 70 °C (Reaction (4)).



The system based on persulfate with multiple activators (heat/UV-LED/ilmenite) improves the overall mineralization degree (Fig. 3), reaching TOC conversion close to 96% under the optimum experimental conditions (Reaction (7)). This is explained by the reduction of Fe(III) to Fe(II) by means of photolysis using UV-LED radiation over ilmenite surface (Eq. (9)) [19] leading to an increase of PS decomposition into SO_4^{2-} . This was confirmed by XPS analysis of the ilmenite surface after 3 h UV-LED irradiation without PS (Fig. S2). The results reveal an increase of $Fe(II)/Fe(III)$ ratio from 40/60 to 52/48. In addition, photo reduction of Fe(III) to Fe(II) produces additional HO^\bullet (Eq. (10)), enhancing the mineralization degree [21]. The presence and contribution of both radicals (SO_4^{2-} and HO^\bullet) was confirmed by using EtOH and TBA [45] as scavengers. The results indicated that SO_4^{2-} was the predominant radical species on the decolorization of DB3 in UV-LED/ilmenite/persulfate system (Fig. S3).

For the sake of comparison, results obtained by combining PS/TiO₂ (Reaction (9)) and PS/UV-LED/TiO₂ (Reaction (10)) are also included. Previous adsorption studies over TiO₂ led to a TOC reduction around 18% (Reaction (8)). Therefore, under the operating conditions used in this work, TiO₂ slightly activates PS whereas, in the presence of UV-LED, the efficiency significantly increases due to the electron/hole pair caused by irradiating the TiO₂ (Eq. (11)) that evolves to the generation of radical species (O_2^{2-} , HO_2^\bullet and HO^\bullet) which are responsible for dye oxidation [46].



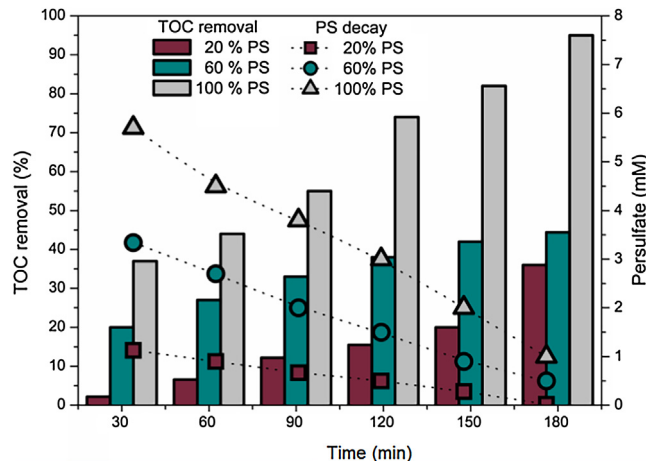
The values of the rate constants obtained by assuming a pseudo-first-order kinetic model confirm the synergistic effect of combining multiple activators (Table 1). This was also corroborated by the apparent activation energy (E_A) (Fig. S4) for PS/UV-LED/Ilmenite process: 51 kJ mol⁻¹. It must be noted that this value is almost three times lower than the E_A reported by Devi et al., to heat-activation of PS: 140 kJ mol⁻¹ [47] and it is also lower than the E_A reported to iron-activated persulfate: 62 kJ mol⁻¹ [48]. Also Zhao et al. [49] reported $E_A: 66 \text{ kJ mol}^{-1}$ for the system based on Fe_3O_4 activated persulfate when the temperature increased from 15 to 55 °C by the oxidation of *p*-nitroaniline.

Fig. 4 illustrates the TOC decay in the presence of different initial PS concentrations, ranging from 20% (0.34 g L⁻¹) to 100% (1.7 g L⁻¹) at 70 °C using 320 mg L⁻¹ ilmenite. As can be observed, the mineralization of DB3 increased around 60% when the dosage of persulfate increased from 20% to 100%. The initial PS concentration is obviously another key point to determine the efficiency of the process. To assess the PS conversion we have quantified the PS yield (ϵ) defined as the amount of TOC converted per unit weight of PS fed [50]. The theoretical maximum value of ϵ at complete TOC conversion when using the stoichiometric PS would be 33.5 mg TOC/g PS. Table 2 shows the values of ϵ after 180 min. For the sake of comparison, results obtained by different ilmenite concentration are also included (the mineralization efficiency between 300 mg L⁻¹ and 450 mg L⁻¹ ilmenite was found to be lower than 5% time and lesser amounts not increase the reaction rate after 180 min reaction).

As can be observed, the increasing of either the ilmenite concentration, reaction temperature or persulfate dose significantly

Table 2Values of ϵ at different operating parameters ($[DB3]_0: 80 \text{ mg L}^{-1}$).

Ilmenite (mg)			Stoichiometric PS (%)			Temperature (°C)			
$[\text{PS}]_0 = 100\% \text{ at } 70^\circ\text{C}$			$[\text{FeTiO}_3]_0 = 320 \text{ mg L}^{-1} \text{ at } 70^\circ\text{C}$			$[[\text{PS}]_0 = 100\%; [\text{FeTiO}_3]_0 = 320 \text{ mg L}^{-1}$			
150	320	450	20	60	100	30	50	70	
ϵ	22.2	31.6	32.7	12.2	25	32.2	10.2	18.7	32.2

 $\epsilon = \text{mg TOC converted/g PS fed.}$ **Fig. 4.** Time evolution of TOC removal and PS converted under UV-LED radiation at 70°C (a). Experimental Conditions: $[DB3]_0 = 80 \text{ mg L}^{-1}$, $[\text{PS}] = 20\text{--}100\%$, $[\text{FeTiO}_3]_0 = 320 \text{ mg L}^{-1}$ and $\text{pH}_0 = 3$.

increases the ϵ values. This implies a faster PS decomposition into SO_4^{2-} , which enhances mineralization. It must be underline that those values are quite close to the theoretical maximum value of ϵ , confirming the absence of scavenging reactions.

The residual TOC (around 1.8 mg L^{-1}) corresponds to traces of formic acid (Fig. S5) as well as a very small amount of non-identified aromatic intermediates (Fig. S6), being the ecotoxicity of the effluent almost negligible to the *A. salina* nauplii (Fig. S7). During the early oxidation stages, 1-amino-4-(methylamino) anthracene-9,10-dione with m/z 252 was identified using GC-MS, probably generated by homolytic rupture of C–N bond [51]. Similar results were reported by Salazar et al. [52] using solar photoelectro-Fenton in the presence of Fe^{2+} and Cu^{2+} to DB3 degradation. This intermediate products evolved to generate phthalic acid that could be oxidized up to oxalic and formic acids [53].

4.1. Catalyst deactivation

To learn on the stability of the catalyst, three successive runs were carried out using the recovered ilmenite under the optimum experimental conditions. The results obtained after each use were compared with those achieved by heat-activated PS in absence of ilmenite. As can be observed in Fig. 5a, the mineralization of DB3 gradually decreased from 43% higher than the obtained by heat-activated PS (1st run) to 23% (2nd run) and negligible activity upon the third run (mineralization <5%). This is a consequence of the lower PS decomposition. Therefore, the values of ϵ decreased after second and third reuse, about 75% and 55% of the theoretical maximum value (ϵ), respectively. The loss of iron from the catalyst by leaching would be one possible cause of deactivation. However, the leached iron (measured by ICP) varied from 0.8 to 0.34 mg L^{-1} after three runs (less than 1% of the total iron contained in the catalyst). Besides, the weight percentage of Fe and Ti decreased less than 5 wt% (measured by TXRF). On the contrary, the XRD spectra (Fig. 1) showed variations in ilmenite phase from 85 to 72.35 after three

uses, respectively, in relation to rutile phase. In addition, new peaks at 20.3° and 26° in XRD spectra after third uses were observed. According to JCPDS Powder Diffraction File (04-008-6818), those peaks could correspond to FeSO_4 [54] and $\text{Fe}_2(\text{SO}_4)_3$ [55] respectively that is in agreement with catalyst deactivation due to SO_4^{2-} deposited on ilmenite surface. Furthermore, the new peak at 44° could be attributed to the Fe_3O_4 and FeOOH formation as the result of corrosion promotion [56,57].

Concerning the XPS of the $\text{Fe} 2\text{p}$ spectrum before third use (Fig. 5b), the presence of a band at 710 eV (peak 1) and another at 724 eV (peak 3) corresponds to $\text{Fe}(\text{II})$. The bands centred at 712 (peak 2) and 725 eV (peak 4) corresponds to $\text{Fe}(\text{III})$. Moreover, a satellite peak of $\text{Fe}(\text{III})$ is shown at 719 eV (peak 5). The percentage of $\text{Fe}(\text{II})$ in ilmenite after UV-LED radiation without PS. XPS of the $\text{Fe} 2\text{p}$ spectrum after use showed at displayed toward higher binding energies. In this case, peak 2 associated to $\text{Fe}(\text{II})$ appeared at 711 eV and peak 2 associated to $\text{Fe}(\text{III})$ at a binding energy of 716 eV [58,59]. The fitting peaks of ilmenite before use indicated the surface amounts of 40/60 for $\text{Fe}(\text{II})/\text{Fe}(\text{III})$. However, in the case of the ilmenite after use the surface amounts were 33/67 for $\text{Fe}(\text{II})/\text{Fe}(\text{III})$. In addition, the peak at 711 can be ascribed to the presence of iron sulfate generated on the ilmenite surface. Al-Shamsi and Thomson [60] detected FeSO_4 at a binding energy of 711.1 eV in the iron spectra ($\text{Fe}2\text{p}$) on deactivated nZVI surface exposed to persulfate. Descotes et al. [61] showed that $\text{Fe}(\text{II})$ and $\text{Fe}(\text{III})$ oxides (FeSO_4 , $\text{Fe}_2(\text{SO}_4)_3$, Fe_2O_3) were formed on oxidized pyrite surfaces in different chemical conditions at 711.55 eV .

4.2. DFT calculation procedure for surface functionalization due to SO_4^{2-} molecule

The aforementioned results suggest the formation of a sulfate passivation layer on the catalyst surface as the most plausible cause of deactivation. In fact, during experiments in highly oxidative conditions, the presence of the SO_4^{2-} can be considered as a powerful tool to functionalize the surface of FeTiO_3 . To check this assumption, we appealed for density functional theory (DFT) calculations. Based on the previous results obtained from scanning tunneling microscopy (STM) investigation of the (0001) ilmenite surface [62], our calculation model consists of a unit cell of ilmenite with surfaces terminated in Fe or Ti atom, where one SO_4^{2-} molecule is placed close to the surface. After the relaxations of super-cell, the optimized structures show that the SO_4^{2-} molecule is adsorbed by a Fe/Ti surface atom on the pristine FeTiO_3 . The minor distance between SO_4^{2-} and Ti atom is about 1.96 \AA and 2.03 \AA between SO_4^{2-} and Fe atom. Two O atoms from SO_4^{2-} molecule are bound to Fe and Ti atom for both surface terminations (see Fig. 6a and b).

In order to study the effect of SO_4^{2-} on FeTiO_3 surface, we have calculated the projected density of states (PDOS) of FeTiO_3 and $\text{SO}_4^{2-}/\text{FeTiO}_3$ for Fe and Ti termination. For comparison, we also show PDOS of pristine FeTiO_3 . These results are presented in Fig. 7. It is known that even though the DFT-GGA method underestimates band gaps of semiconductors and insulators, it does give though reliable band widths and shapes. In this work, we focus on comparison of the interaction of SO_4^{2-} on FeTiO_3 surface. The PDOS for pristine FeTiO_3 of Fe, Ti and O atom are shown in Fig. 7(a). We set the

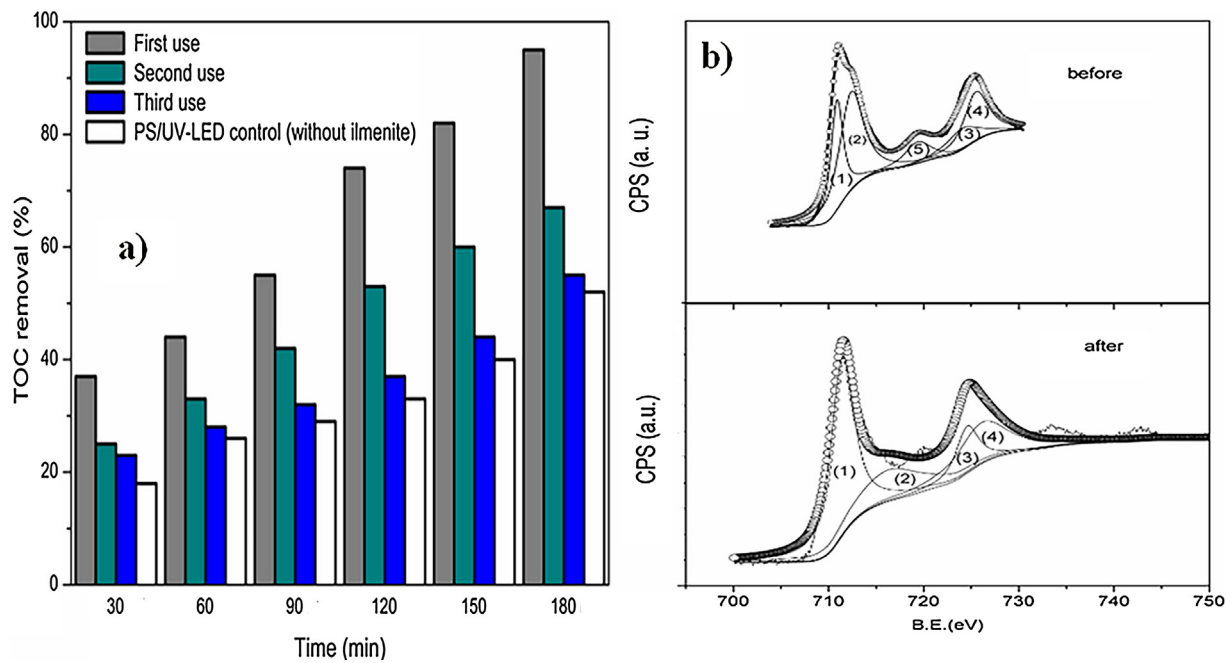


Fig. 5. Reuse of ilmenite in the repeated DB3 mineralization experiment (a). XPS spectra of Fe2p for ilmenite before and after use. Experimental Conditions: $[DB3]_0 = 80 \text{ mg L}^{-1}$, $[PS]_0 = 100\%$, $T = 70^\circ\text{C}$ and $pH_0 = 3$.

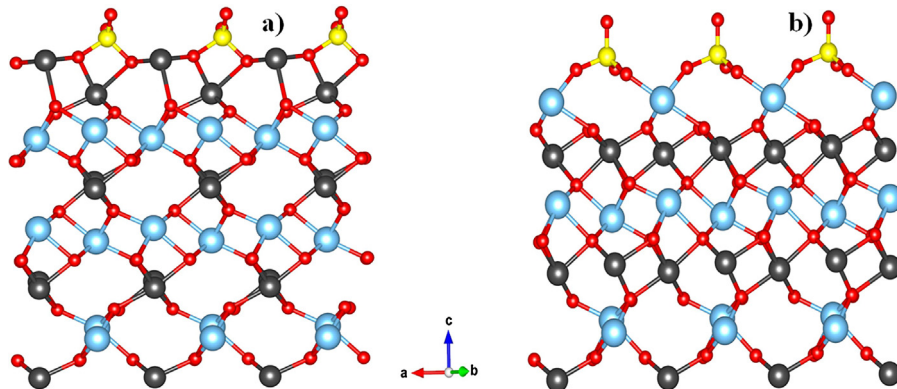


Fig. 6. Crystal structure of FeTiO₃ ilmenite + SO₄²⁻ (Fe surface) and (b) FeTiO₃ + SO₄²⁻ (Ti surface). Ti (blue), Fe (black), O (red) and SO₄²⁻ (yellow). (For interpretation of the references to colour in this figure legend, the reader is referred to the web version of this article.)

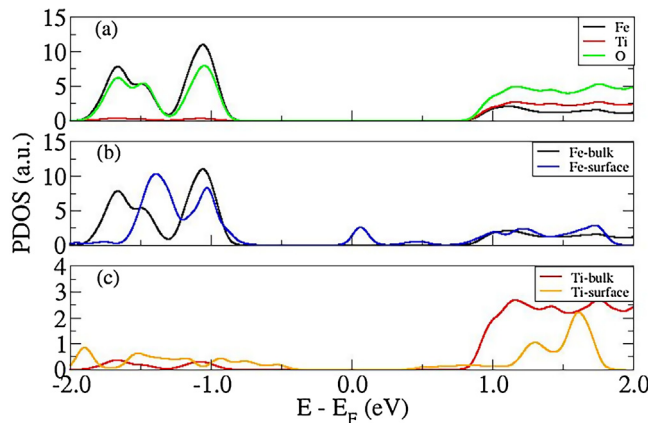


Fig. 7. Comparison of projected total density of states (PDOS) for pristine FeTiO₃ (a), FeTiO₃ + SO₄²⁻ (Fe-surface) (b) and FeTiO₃ + SO₄²⁻ (Ti surface) (c). The Fermi energy is referenced at 0 eV.

Fermi energy to 0 eV. In the case of SO₄²⁻/FeTiO₃(Fe-termination), a new remarkable peak appear around the Fermi energy as a result of the SO₄²⁻ adsorption (Fig. 7(b)). As one can be seen from Fig. 7(c), the PDOS of SO₄²⁻/FeTiO₃(Ti-termination) in this region is the similar to that of pristine FeTiO₃.

We compute the charge transfer (CT), between SO₄²⁻ molecule and FeTiO₃, using the Bader charge analysis method [63] with the code developed by the Henkelman's group [64]. The amount of charge transfer between SO₄²⁻ and Fe atoms is about 1.3 electrons from Fe to the SO₄²⁻ molecule and 1.45 electrons from Ti to the SO₄²⁻ molecule. These results show that the slightly increment of the proportion Fe(III)/Fe(II) experimentally observed can be due to the adsorption of SO₄²⁻ on the FeTiO₃ surface.

5. Conclusion

The irradiation with UV-LED ($\lambda: 405 \text{ nm}$) allows overcoming the drawbacks associated with the use of natural ilmenite (FeTiO₃) to activate persulfate. The combined UV-LED/ilmenite/PS show synergistic effect compared to the individual processes, achieving DB3

mineralization around 95% under the optimum operating conditions (320 mg L^{-1} of ilmenite, $\text{pH}_0:3$ using 100% of stoichiometric amount of PS at 70°C under UV-LED radiation). Despite the negligible iron leaching, the catalyst suffered a dramatically loss of activity after three consecutive runs due to the interaction between SO_4^{2-} and the surface of FeTiO_3 . This assumption (confirmed by DFT calculation) entails the formation of a passivation layer on the surface that also justifies the slightly increment of the proportion $\text{Fe(III)}/\text{Fe(II)}$ experimentally observed.

Acknowledgements

Comunidad Autónoma de Madrid and MINECO have supported this work through projects S2013/MAE-2716 and CTQ2013-41963-R, respectively. Jefferson E. Silveira and Wendel S. Paz gratefully acknowledges the support from CAPES: Science Without Borders Program, Ministry of Education Brazil, under grant BEX-1046/13-6 and BEX-9476/13-0 respectively.

Appendix A. Supplementary data

Supplementary data associated with this article can be found, in the online version, at <http://dx.doi.org/10.1016/j.apcatb.2017.07.072>.

References

- [1] X. Florenza, A.M.S. Solano, F. Centellas, C.A. Martínez-Huitle, E. Brillas, S. García-Segura, Degradation of the azo dye Acid Red 1 by anodic oxidation and indirect electrochemical processes based on Fenton's reaction chemistry. Relationship between decolorization, mineralization and products, *Electrochim. Acta* 142 (2014) 276–288, <http://dx.doi.org/10.1016/j.electacta.2014.07.117>.
- [2] S.S. Ashraf, M.A. Rauf, S. Alhadrami, Degradation of Methyl Red using Fenton's reagent and the effect of various salts, *Dye Pigments* 69 (2006) 74–78, <http://dx.doi.org/10.1016/j.dyepig.2005.02.009>.
- [3] V. Khandegar, A.K. Saroha, Electrocoagulation for the treatment of textile industry effluent—a review, *J. Environ. Manage.* 128 (2013) 949–963, <http://dx.doi.org/10.1016/j.jenvman.2013.06.043>.
- [4] S. García-Segura, E. Brillas, Combustion of textile monoazo, diazo and triazo dyes by solar photoelectro-Fenton: decolorization, kinetics and degradation routes, *Appl. Catal. B: Environ.* 181 (2016) 681–691, <http://dx.doi.org/10.1016/j.apcatb.2015.08.042>.
- [5] F.C. Moreira, S. García-Segura, V.J.P. Vilar, R.A.R. Boaventura, E. Brillas, Decolorization and mineralization of Sunset Yellow FCF azo dye by anodic oxidation, electro-Fenton, UVA photoelectro-Fenton and solar photoelectro-Fenton processes, *Appl. Catal. B: Environ.* 142–143 (2013) 877–890, <http://dx.doi.org/10.1016/j.apcatb.2013.03.023>.
- [6] A. El-Ghennamy, F. Centellas, J.A. Garrido, R.M. Rodríguez, I. Sirés, P.L. Cabot, E. Brillas, Decolorization and mineralization of Orange G azo dye solutions by anodic oxidation with a boron-doped diamond anode in divided and undivided tank reactors, *Electrochim. Acta* 130 (2014) 568–576, <http://dx.doi.org/10.1016/j.electacta.2014.03.066>.
- [7] A. Thiam, I. Sirés, F. Centellas, P.L. Cabot, E. Brillas, Decolorization and mineralization of Allura Red AC azo dye by solar photoelectro-Fenton: identification of intermediates, *Chemosphere* 136 (2015) 1–8, <http://dx.doi.org/10.1016/j.chemosphere.2015.03.047>.
- [8] D. Rajamanickam, M. Shanthi, Photocatalytic degradation of an azo dye Sunset Yellow under UV-A light using TiO_2/CAC composite catalysts, *Spectrochim. Acta—Part A: Mol. Biomol. Spectrosc.* 128 (2014) 100–108, <http://dx.doi.org/10.1016/j.saa.2014.02.126>.
- [9] F.D. Castro, J.P. Bassin, M. Dezotti, Treatment of a simulated textile wastewater containing the Reactive Orange 16 azo dye by a combination of ozonation and moving-bed biofilm reactor: evaluating the performance, toxicity, and oxidation by-products, *Environ. Sci. Pollut. Res.* (2016) 1–10, <http://dx.doi.org/10.1007/s11356-016-7119-x>.
- [10] S.-Y. Oh, H.-W. Kim, J.-M. Park, H.-S. Park, C. Yoon, Oxidation of polyvinyl alcohol by persulfate activated with heat, Fe^{2+} , and zero-valent iron, *J. Hazard. Mater.* 168 (2009) 346–351, <http://dx.doi.org/10.1016/j.jhazmat.2009.02.065>.
- [11] A. Asghar, A.A.A. Raman, W.M.A.W. Daud, Advanced oxidation processes for in-situ production of hydrogen peroxide/hydroxyl radical for textile wastewater treatment: a review, *J. Clean. Prod.* 87 (2015) 826–838, <http://dx.doi.org/10.1016/j.jclepro.2014.09.010>.
- [12] Z. Frontistis, E. Hapeshi, D. Fatta-Kassinos, D. Mantzavinos, Ultraviolet-activated persulfate oxidation of methyl orange: a comparison between artificial neural networks and factorial design for process modelling, *Photochem. Photobiol. Sci.* 14 (2015) 528–535, <http://dx.doi.org/10.1039/c4pp00277f>.
- [13] S.A. Kordkandi, M. Forouzesh, Application of full factorial design for methylene blue dye removal using heat-activated persulfate oxidation, *J. Taiwan Inst. Chem. Eng.* 45 (2014) 2597–2604, <http://dx.doi.org/10.1016/j.jtice.2014.06.015>.
- [14] X.R. Xu, X.Z. Li, Degradation of azo dye Orange G in aqueous solutions by persulfate with ferrous ion, *Sep. Purif. Technol.* 72 (2010) 105–111, <http://dx.doi.org/10.1016/j.seppur.2010.01.012>.
- [15] A.L. Teel, M. Ahmad, R.J. Watts, Persulfate activation by naturally occurring trace minerals, *J. Hazard. Mater.* 196 (2011) 153–159, <http://dx.doi.org/10.1016/j.jhazmat.2011.09.011>.
- [16] P. García-Muñoz, G. Pliego, J.A. Zazo, A. Bahamonde, J.A. Casas, Ilmenite (FeTiO_3) as low cost catalyst for advanced oxidation processes, *J. Environ. Chem. Eng.* 4 (2016) 542–548, <http://dx.doi.org/10.1016/j.jece.2015.11.037>.
- [17] Y.H. Chen, Synthesis, characterization and dye adsorption of ilmenite nanoparticles, *J. Non Cryst. Solids* 357 (2011) 136–139, <http://dx.doi.org/10.1016/j.jnoncrysol.2010.09.070>.
- [18] A. Mehdilo, M. Irannajad, B. Rezai, Chemical and mineralogical composition of ilmenite: effects on physical and surface properties, *Miner. Eng.* 70 (2015) 64–76, <http://dx.doi.org/10.1016/j.mineng.2014.09.002>.
- [19] P. García-Muñoz, G. Pliego, J.A. Zazo, B. Barbero, A. Bahamonde, J.A. Casas, Modified ilmenite as catalyst for CWPO-photoassisted process under LED light, *Chem. Eng. J.* 318 (2016) 89–94, <http://dx.doi.org/10.1016/j.cej.2016.05.093>.
- [20] M. Munoz, P. Domínguez, Z.M. de Pedro, J.A. Casas, J.J. Rodriguez, Naturally-occurring iron minerals as inexpensive catalysts for CWPO, *Appl. Catal. B: Environ.* 203 (2017) 166–173, <http://dx.doi.org/10.1016/j.apcatb.2016.10.015>.
- [21] J.A. Zazo, G. Pliego, P. García-Muñoz, J.A. Casas, J.J. Rodriguez, UV-LED assisted catalytic wet peroxide oxidation with a $\text{Fe(II)}-\text{Fe(III)}$ -activated carbon catalyst, *Appl. Catal. B: Environ.* 192 (2016) 350–356, <http://dx.doi.org/10.1016/j.apcatb.2016.04.010>.
- [22] C. Liang, C.J. Bruell, M.C. Marley, K.L. Sperry, Persulfate oxidation for in situ remediation of TCE. I. Activated by ferrous ion with and without a persulfate-thiosulfate redox couple, *Chemosphere* 55 (2004) 1213–1223, <http://dx.doi.org/10.1016/j.chemosphere.2004.01.029>.
- [23] O. Tokode, R. Prabhu, L.A. Lawton, P.K.J. Robertson, The effect of pH on the photonic efficiency of the destruction of methyl orange under controlled periodic illumination with UV-LED sources, *Chem. Eng. J.* 246 (2014) 337–342, <http://dx.doi.org/10.1016/j.cej.2014.03.002>.
- [24] M.H. Rasolifard, M. Fazli, M.R. Eskandarian, Performance of the light-emitting-diodes in a continuous photoreactor for degradation of Direct Red 23 using UV-LED/ $\text{S}_2\text{O}_8^{2-}$ process, *J. Ind. Eng. Chem.* 24 (2013) 121–126, <http://dx.doi.org/10.1016/j.jiec.2014.09.018>.
- [25] Č. Novotný, N. Dias, A. Kapanan, K. Malachová, M. Vádrovová, M. Itávára, N. Lima, Comparative use of bacterial, algal and protozoan tests to study toxicity of azo- and anthraquinone dyes, *Chemosphere* 63 (2006) 1436–1442, <http://dx.doi.org/10.1016/j.chemosphere.2005.10.002>.
- [26] M.D. Hernández-alonso, E. Mena, A. Rey, P. García-mu, WO_3-TiO_2 based catalysts for the simulated solar radiation assisted photocatalytic ozonation of emerging contaminants in a municipal wastewater treatment plant effluent, *Appl. Catal. B: Environ.* 155 (2014) 274–284, <http://dx.doi.org/10.1016/j.apcatb.2014.02.035>.
- [27] P. Giannozzi, S. Baroni, N. Bonini, M. Calandra, R. Car, C. Cavazzoni, D. Ceresoli, G.L. Chiarotti, M. Cococcioni, I. Dabo, A. Dal Corso, S. de Gironcoli, S. Fabris, G. Fratesi, R. Gebauer, U. Gerstmann, C. Gougoussis, A. Kokalj, M. Lazzeri, L. Martin-Samios, N. Marzari, F. Mauri, R. Mazzarello, S. Paolini, A. Pasquarello, L. Paulatto, C. Sbraccia, S. Scandolo, G. Scaluzero, A.P. Seitsonen, A. Smogunov, P. Umari, R.M. Wentzcovitch, QUANTUM ESPRESSO: a modular and open-source software project for quantum simulations of materials, *J. Phys. Condens. Matter.* 21 (2009) 395502, <http://dx.doi.org/10.1088/0953-8984/21/39/395502>.
- [28] J.P. Perdew, K. Burke, M. Ernzerhof, Generalized gradient approximation made simple, *Phys. Rev. Lett.* 77 (1996) 3865–3868, <http://dx.doi.org/10.1103/PhysRevLett.77.3865>.
- [29] A.V. Krukau, O.A. Vydróv, A.F. Izmaylov, G.E. Scuseria, A. Krukau V, O.A. Vydróv, A.F. Izmaylov, G.E. Scuseria, Influence of the exchange screening parameter on the performance of screened hybrid functionals Influence of the exchange screening parameter on the performance of screened hybrid functionals, *J. Chem. Phys.* 224106 (2006), <http://dx.doi.org/10.1063/1.2404663>.
- [30] J. Heyd, J.E. Peralta, G.E.S.L. Martin, J. Heyd, J.E. Peralta, G.E. Scuseria, R.L. Martin, Energy band gaps and lattice parameters evaluated with the Heyd-Scuseria-Ernzerhof screened hybrid functional Energy band gaps and lattice parameters evaluated with the Heyd-Scuseria-Ernzerhof screened hybrid functional, *J. Chem. Phys.* 174101 (2012), <http://dx.doi.org/10.1063/1.2085170>.
- [31] B.G. Janesko, T.M. Henderson, G.E. Scuseria, T.M. Henderson, Screened hybrid density functionals for solid-state chemistry and physics, *Phys. Chem. Chem. Phys.* (2009) 443–454, <http://dx.doi.org/10.1039/b812838c>.
- [32] N. Troullier, J.L. Martins, Efficient pseudopotentials for plane-wave calculations. II. Operators for fast iterative diagonalization, *Phys. Rev. B* 43 (1991) 8861–8869, <http://dx.doi.org/10.1103/PhysRevB.43.8861>.
- [33] B.A. Wechsler, C.T. Prewitt, Crystal structure of ilmenite (FeTiO_3) at high temperature and at high pressure, *Am. Mineral.* 69 (1984) 176–185.

[34] G. Pliego, J.A. Zazo, S. Blasco, J.J. Casas, Treatment of highly polluted hazardous industrial wastewaters by combined coagulation-adsorption and high-temperature fenton oxidation, *Ind. Eng. Chem. Res* 51 (2012) 2888–2896, <http://dx.doi.org/10.1021/ie202587b>.

[35] C. Liang, C.-F. Huang, N. Mohanty, R.M. Kurakalva, A rapid spectrophotometric determination of persulfate anion in ISCO, *Chemosphere* 73 (2008) 1540–1543, <http://dx.doi.org/10.1016/j.chemosphere.2008.08.043>.

[36] P. Vanhaecke, G. Persoone, C. Claus, P. Sorgeloos, Proposal for a short-term toxicity test with *Artemia nauplii*, *Ecotoxicol. Environ. Saf.* 5 (1981) 382–387, [http://dx.doi.org/10.1016/0147-6513\(81\)90012-9](http://dx.doi.org/10.1016/0147-6513(81)90012-9).

[37] a. T. Raghavender, N. Hoa Hong, K. Joon Lee, M.H. Jung, Z. Skoko, M. Vasilevskiy, M.F. Cerqueira, a. P. Samantilleke, Nano-ilmenite FeTiO_3 : synthesis and characterization, *J. Magn. Magn. Mater.* 331 (2013) 129–132, <http://dx.doi.org/10.1016/j.jmmm.2012.11.028>.

[38] M. Charilaou, D. Sheptyakov, J.F. Löffler, A.U. Gehring, Large spontaneous magnetostriiction in FeTiO_3 and adjustable magnetic configuration in Fe(III)-doped FeTiO_3 , *Phys. Rev. B: Condens. Matter Mater. Phys.* 86 (2012) 1–11, <http://dx.doi.org/10.1103/PhysRevB.86.024439>.

[39] R.H. Waldemer, P.G. Tratnyek, R.L. Johnson, J.T. Nurmi, Oxidation of chlorinated ethenes by heat-activated persulfate: kinetics and products, *Environ. Sci. Technol.* 41 (2007) 1010–1015 <http://www.ncbi.nlm.nih.gov/pubmed/17328217>.

[40] M. Zhang, X. Chen, H. Zhou, M. Muruganathan, Y. Zhang, Degradation of *p*-nitrophenol by heat and metal ions co-activated persulfate, *Chem. Eng. J.* 264 (2015) 39–47, <http://dx.doi.org/10.1016/j.cej.2014.11.060>.

[41] J. Yan, L. Han, W. Gao, S. Xue, M. Chen, Biochar supported nanoscale zerovalent iron composite used as persulfate activator for removing trichloroethylene, *Bioproc. Technol.* 175 (2015) 269–274, <http://dx.doi.org/10.1016/j.bioproc.2014.10.103>.

[42] Y.C. Lee, S.L. Lo, J. Kuo, Y.L. Lin, Persulfate oxidation of perfluoroctanoic acid under the temperatures of 20–40 °C, *Chem. Eng. J.* 198–199 (2012) 27–32, <http://dx.doi.org/10.1016/j.cej.2012.05.073>.

[43] J.M. Monteagudo, A. Durán, R. González, A.J. Expósito, In situ chemical oxidation of carbamazepine solutions using persulfate simultaneously activated by heat energy, UV, light, Fe^{2+} ions, and H_2O_2 , *Appl. Catal. B: Environ.* 176–177 (2015) 120–129, <http://dx.doi.org/10.1016/j.apcatb.2015.03.055>.

[44] J. Saïen, Z. Ojaghloo, a. R. Soleymani, M.H. Rasouliard, Homogeneous and heterogeneous AOPs for rapid degradation of Triton X-100 in aqueous media via UV light, nano titania hydrogen peroxide and potassium persulfate, *Chem. Eng. J.* 167 (2011) 172–182, <http://dx.doi.org/10.1016/j.cej.2010.12.017>.

[45] G.P. Anipsitakis, D.D. Dionysiou, Radical generation by the interaction of transition metals with common oxidants radical generation by the interaction of transition metals with common oxidants, *Environ. Sci. Technol.* (2004) 3705–3712, <http://dx.doi.org/10.1021/es035121o>.

[46] W.K. Jo, R.J. Tayade, Recent developments in photocatalytic dye degradation upon irradiation with energy-efficient light emitting diodes, *Cuihua Xuebao/Chin. J. Catal.* 35 (2014) 1781–1792, [http://dx.doi.org/10.1016/S1872-2067\(14\)60205-9](http://dx.doi.org/10.1016/S1872-2067(14)60205-9).

[47] P. Devi, U. Das, A.K. Dalai, In-situ chemical oxidation: principle and applications of peroxide and persulfate treatments in wastewater systems, *Sci. Total Environ.* 571 (2016) 643–657, <http://dx.doi.org/10.1016/j.scitotenv.2016.07.032>.

[48] A. Romero, A. Santos, F. Vicente, C. González, Diuron abatement using activated persulphate: effect of pH, $\text{Fe}(\text{II})$ and oxidant dosage, *Chem. Eng. J.* 162 (2010) 257–265, <http://dx.doi.org/10.1016/j.cej.2010.05.044>.

[49] Y.S. Zhao, C. Sun, J.Q. Sun, R. Zhou, Kinetic modeling and efficiency of sulfate radical-based oxidation to remove *p*-nitroaniline from wastewater by persulfate/ Fe_3O_4 nanoparticles process, *Sep. Purif. Technol.* 142 (2015) 182–188, <http://dx.doi.org/10.1016/j.seppur.2014.12.035>.

[50] J.A. Zazo, G. Pliego, S. Blasco, J.A. Casas, J.J. Rodriguez, Intensification of the Fenton process by increasing the temperature, *Ind. Eng. Chem. Res.* 50 (2011) 866–870, <http://dx.doi.org/10.1021/ie101963k>.

[51] H.Z. Zhao, Y. Sun, L.N. Xu, J.R. Ni, Removal of Acid Orange 7 in simulated wastewater using a three-dimensional electrode reactor: removal mechanisms and dye degradation pathway, *Chemosphere* 78 (2010) 46–51, <http://dx.doi.org/10.1016/j.chemosphere.2009.10.034>.

[52] R. Salazar, E. Brillas, I. Sirés, Finding the best $\text{Fe}^{2+}/\text{Cu}^{2+}$ combination for the solar photoelectro-Fenton treatment of simulated wastewater containing the industrial textile dye Disperse Blue 3, *Appl. Catal. B: Environ.* 115–116 (2012) 107–116, <http://dx.doi.org/10.1016/j.apcatb.2011.12.026>.

[53] J.M. Fanchiang, D.H. Tseng, Degradation of anthraquinone dye C.I. Reactive Blue 19 in aqueous solution by ozonation, *Chemosphere* 77 (2009) 214–221, <http://dx.doi.org/10.1016/j.chemosphere.2009.07.038>.

[54] M. Kim, Y. Jung, B. Kang, High electrochemical performance of 3.9 V LiFeSO_4F directly synthesized by a scalable solid-state reaction within 1 h, *J. Mater. Chem. A: Mater. Energy Sustain.* 3 (2015) 7583–7590, <http://dx.doi.org/10.1039/C4TA07095j>.

[55] N. Recham, J.-N. Chotard, L. Dupont, C. Delacourt, W. Walker, M. Armand, J.-M. Tarascon, A 3.6 V lithium-based fluorosulphate insertion positive electrode for lithium-ion batteries, *Nat. Mater.* 9 (2010) 68–74, <http://dx.doi.org/10.1038/nmat2590>.

[56] Y. Hou, Z. Xu, S. Sun, Controlled synthesis and chemical conversions of FeO nanoparticles, *Angew. Chem. Int. Ed.* 46 (2007) 6329–6332, <http://dx.doi.org/10.1002/anie.200701694>.

[57] T. Wang, J. Su, X. Jin, Z. Chen, M. Megharaj, R. Naidu, Functional clay supported bimetallic nZVI/Pd nanoparticles used for removal of methyl orange from aqueous solution, *J. Hazard. Mater.* 262 (2013) 819–825, <http://dx.doi.org/10.1016/j.jhazmat.2013.09.028>.

[58] T. Yamashita, P. Hayes, Analysis of XPS spectra of Fe^{2+} and Fe^{3+} ions in oxide materials, *Appl. Surf. Sci.* 254 (2008) 2441–2449, <http://dx.doi.org/10.1016/j.apsusc.2007.09.063>.

[59] H. Search, C. Journals, A. Contact, M. Iopscience, I.P. Address, A study of the core level electrons in iron and its three oxides by means of x-ray photoelectron spectroscopy, *J. Phys. D: Appl. Phys.* 16 (1983) 723–732, <http://dx.doi.org/10.1088/0022-3727/16/5/005>.

[60] M.A. Al-Shamsi, N.R. Thomson, Treatment of organic compounds by activated persulfate using nanoscale zerovalent iron, *Ind. Eng. Chem. Res.* 52 (2013) 13564–13571, <http://dx.doi.org/10.1021/ie400387p>.

[61] M. Descotes, F. Mercier, N. Thromat, C. Beaucaire, M. Gautier-Soyer, Use of XPS in the determination of chemical environment and oxidation state of iron and sulfur samples: constitution of a data basis in binding energies for Fe and S reference compounds and applications to the evidence of surface species of an oxidized py, *Appl. Surf. Sci.* 165 (2000) 288–302, [http://dx.doi.org/10.1016/S0169-4332\(00\)00443-8](http://dx.doi.org/10.1016/S0169-4332(00)00443-8).

[62] R.A. Fellows, A.R. Lennie, A.W. Munz, D.J. Vaughan, G. Thornton, Structures of FeTiO_3 (0001) surfaces observed by scanning tunneling microscopy, *Am. Mineral.* 84 (1999) 1384 <http://ammin.geoscienceworld.org/cgi/content/abstract/84/9/1384>.

[63] R.F.W. Bader, Atoms in molecules, *Acc. Chem. Res.* 18 (1985) 9–15, <http://dx.doi.org/10.1021/ar00109a003>.

[64] G. Henkelman, A. Arnaldsson, H. Jónsson, A fast and robust algorithm for Bader decomposition of charge density, *Comput. Mater. Sci.* 36 (2006) 354–360, <http://dx.doi.org/10.1016/j.commatsci.2005.04.010>.